Ultramicroscopy 251 (2023) 113770

Contents lists available at ScienceDirect

Ultramicroscopy

journal homepage: www.elsevier.com/locate/ultramic

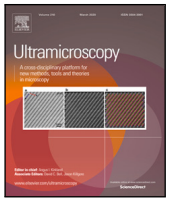

A correction for higher-order refraction in cathodoluminescence spectrometry

Michael Stöger-Pollach [a,b,*], Keanu Zenz [b], Felix Ursin [b], Johannes Schilberg [b], Leo Stöger [b]

[a] University Service Center for Transmission Electron Microscopy (USTEM), Technische Universität Wien, Wiedner Hauptstraße 8-10, 1040 Wien, Austria
[b] Institute of Solid State Physics, Technische Universität Wien, Wiedner Hauptstraße 8-10, 1040 Wien, Austria

ARTICLE INFO

Keywords:
Cathodoluminescence
Transmission electron microscope
Refraction of light

ABSTRACT

Cathodoluminescence (CL) is a developing analytical method in electron microscopy, because of its excellent energy resolution. Usually a Czerny–Turner type spectrometer is employed, having a blazed grating as analyzer. Unlike a prism analyzer, where the dispersion depends on the refractive index of the prism itself leading to a non-linear spectral distribution, the grating has the advantage that the spectral distribution depends linearly on the wavelength. As a draw-back, higher-order refraction alters the measured optical spectrum at larger wavelengths. In general, blazed gratings are used in order to minimize this effect in a certain spectral range. Nevertheless, the higher-order intensities can be still significant. In the present study we present a method for correcting the acquired optical spectra with respect to higher order diffraction intensities and apply it to CaO and GaN CL-spectra.

1. Introduction

There are manifold ways of how an electron beam may interact with a specimen. One of those is the excitation of valence electrons into the conduction band of the probed material. The subsequent de-excitation process results in the emission of a characteristic electromagnetic radiation, which can be in the range of infra-red to visible light, or to ultraviolet radiation [1,2]. The energies of the emitted photons depend on the material, its purity and the presence of defects and is independent of the initial electron energy. Additionally, the de-excitation process itself is independent of the prior valence electron excitation [3]. Such a process is therefore called an *incoherent* light emission process. In opposite, when a swift electron passes through a dielectric medium it first has to adopt its electric field components to the altered dielectric environment directly at the entrance surface. This causes also the emission of radiation [4] being called Transition Radiation (TR). Second, if the velocity of the fast probe electron exceeds the phase velocity of light inside the dielectric medium, another effect causes emission of radiation, too, which is described within the framework of the Čerenkov effect [5]. The latter two emission processes are directly related to the probe electron and its energy and are therefore called *coherent* light emission processes [3]. Anyhow, all of them emit light in the IR–VIS–UV range, dependent on the materials properties.

The goal of any CL measurement is to record the true spectrum being emitted from the sample and in most cases the incoherent part of the spectrum is the one being aimed for. Whereas in the beginning photographic plates were used [6], nowadays optical spectrometers are applied (see for example [7,8]). Some of which are prism spectrometers and others are Czerny-type spectrometers employing analyzing gratings. In order to get the real signal stemming from the specimen, the way the light has to travel until it reaches the detector has to be known exactly. All optical components passed through by the light need to be characterized with high precision. Additionally, the wavelengths dependent properties of the detector have to be known well, which is given by the wavelength dependent detection quantum efficiency (DQE(λ)).

In general a CL system consists of a high-grade polished Aluminum mirror, a focusing lens or a light guide with a certain length being responsible for ensuring that the light beam hits the analyzer as parallel as possible, thus having an influence on the final spectral resolution. The analyzer itself can be an optical prism with a certain refractive index $n(\lambda)$, or it is a blazed grating with a certain lattice parameter and blazing angle. Finally the light is somehow guided towards the detector, where the dispersion of the wavelength strongly depends on the distance from the grating to the detector. When a grating is utilized, higher order diffraction appears and an overlap between the spectral dispersion of the first and second order will appear. The detector is not able to distinguish between different diffraction orders.

* Corresponding author at: University Service Center for Transmission Electron Microscopy (USTEM), Technische Universität Wien, Wiedner Hauptstraße 8-10, 1040 Wien, Austria.
E-mail address: stoeger@ustem.tuwien.ac.at (M. Stöger-Pollach).

https://doi.org/10.1016/j.ultramic.2023.113770
Received 7 October 2022; Received in revised form 12 May 2023; Accepted 26 May 2023
Available online 30 May 2023
0304-3991/© 2023 The Author(s). Published by Elsevier B.V. This is an open access article under the CC BY license (http://creativecommons.org/licenses/by/4.0/).

The following chapters are structured in such a way that first the experimental setup is described. Then the diffraction grating is considered in a close-up, especially with regard to its function as an analyzer. Finally, a software routine that removes the higher diffraction orders is discussed using the example of GaN and the most prominent emission line of Sulfur doped CaO.

2. Experimental set-up

In the present manuscript we make use of a GATAN VULCAN CL detection system consisting of a dedicated sample holder with cooling capabilities, which is designed such, that two mirrors above and below the specimen reflect the light into two light guides. The light then is guided out of the microscope by two connectors mounted on the dedicated holder. At the connectors two optical fibers are mounted guiding the light into the spectrometer, which itself is placed beside the transmission electron microscope (TEM). Two sets of light-guides are available. One is optimized for VIS-nearIR at 400 nm–1380 nm, and the second one covers the nearUV–VIS region being 360 nm–920 nm, respectively. The spectrometer is a Czerny–Turner type spectrometer with an entrance slit being responsible for the size of the illuminated spot on the reflecting diffraction grating and thus being responsible for the resolution of the spectrum. Inside the spectrometer the light is further focused by a concave mirror onto the grating position. One can select between two different gratings, which are in the present case one with 150 lines/mm and a second one with 1200 lines/mm. Both of them have a blazing wavelength of 500 nm. Finally, the dispersed beam is deflected via some collection optics onto a CCD detector.

The grating causes also higher order diffraction maxima of short wavelength light, which partially overlap with lower order but longer wavelength diffraction maxima. Hence, the grating is discussed here in a very detailed close-up in the theory section.

3. Theory

For better illustration, let us first consider the reflection of a parallel beam on a grid of point reflectors at a distance d. Since this case is analogous to diffraction at a transmission grating, the angles under which positive interference occurs and thus result in maxima in the intensity distribution are given by

$$d \cdot \sin(\vartheta_m) = m \cdot \lambda. \tag{1}$$

Where $m \in \mathbb{N}$ describes the order of diffraction. Here, ϑ_0 is the angle into which the largest part of the intensity of the incident beam is directed and results from the reflection law of a plane mirror. If the individual reflectors are tilted by the angle γ against the normal of their arrangement axis, the angle into which the greatest part of the incident intensity is directed also changes by the value of γ. Accordingly, most of the intensity can be directed into the first diffraction order. Instead of Eq. (1), the criterion for positive interference is now

$$d(\sin(\alpha) + \sin(\beta)) = m \cdot \lambda \tag{2}$$

where α is the angle against the grating normal of the incoming light beam and β is the one of the outgoing beam [8]. The distance that can be evaluated at the detector is proportional to the sine of the angle β. It is thus clearly visible that the difference between the distances of two diffraction orders m_1 and m_2, at the detector is proportional to Δm, ($\Delta m = m_2 - m_1$). Furthermore, there is a linear dependence of the product of the sine of the angle of incidence and the distance $\sin(\beta) \cdot d$, i.e. the position of the incidence at the detector (at a fixed angle of incidence α) depends on the product of the wavelength and the diffraction order $\lambda \cdot m$ leading to a dispersion of $x(\lambda)$. The dispersed light is then be projected to the detector via some optics. Thus, in the measurement setup being used, it is actually the intensity at a location on the detector, which we will refer to here as $\xi(\lambda) = x(\lambda) \cdot d/z$, rather than the wavelength λ which is detected by the CCD.

$$\xi(\lambda) = \frac{z}{d} \cdot m \cdot \lambda, \tag{3}$$

where d is the lattice constant of the grating and z denotes the focal length of the coupling optical element between the grating to the detector. The wavelength of higher diffraction orders $m > 1$ thus corresponds to that of the first diffraction order, but is incorrectly recognized as $\lambda_m = m \cdot \lambda$. In a classical blazed grating, the ideal intensity distribution of a monochromatic signal corresponds to the product of a normalized sinc^2 function and the sum of scaled delta comb ($\text{Ш} = \sum_{k=1}^{n} \delta(x - k \cdot x_0)$; k,n $\in \mathbb{N}$) [8]

$$I(\lambda, \xi) = \mathrm{sinc}^2\left(\frac{\xi(\lambda) - n_B \lambda_B}{\lambda}\right) \cdot \frac{1}{\lambda} \cdot \text{Ш}\left(\frac{\xi(\lambda)}{\lambda}\right), \tag{4}$$

Using a grating being blazed for $\lambda_B = 500$ nm means and such that the first order diffraction maximum is the strongest one ($n_B = 1$) causes that higher order diffraction for monochromatic light is totally suppressed, because the sinc^2-function equals zero at $\lambda = n \cdot 500$ nm, with $n \in \{\mathbb{Z} \setminus 1\}$. Incoming light having a wavelength of $\lambda = \lambda_B = 500$ nm is found with its full intensity in the first order diffraction maximum. Higher orders do not show up at all. But for light with $\lambda = (500 \pm \epsilon)$ nm higher diffraction orders still contribute to the overall signal. The smaller being ϵ, the better is the suppression of the intensities in higher order peaks. Still they are not zero. For better understanding we simulated the spectra of monochromatic light falling onto our grating for various wavelengths. We see, that also the envelope function – which is the sinc^2-function – is effected by the chosen wavelength (see Fig. 1).

The x-axis in Fig. 1 is describing the wavelength but in the experimental set-up it is the spatial coordinate ξ of the detector. The wavelength interval in the calculations was chosen such, that it is slightly larger as can be detected with our set-up. In the experiment the limitations are given by the light guide directing the CL-intensities out of the TEM and guiding the light onto the grating and are prior to the analyzer. Their absorption coefficient is such, that we are limited to a range from 380 nm to 1200 nm. Below and above much too much intensity is absorbed by the material of the optical fibers.

Anyhow, light having a wavelength of 380 nm can pass through and has its second-order maximum at 760 nm. Consequently, this is in a range where the first diffraction order of red light also hits the detector. Therefore, there is a mixing of signals of the first and second diffraction order. Fig. 2 shows a calculation for different wavelengths and several diffraction orders. The attenuation for the higher orders is in the range of 80%–98%.

In order to calculate the wavelength dependent efficiency of the grating, we make use of the scalar Kirchhoff diffraction theory. It ignores the vectorial aspect of light but provides results comparable to those obtained by rigorous theory derived directly from Maxwell's equations. The scalar theory is much simpler but is valid only under the limits of $d > 5 \cdot \lambda$ [9–11]. When using the grating with 150 lines/mm, the lattice constant of the analyzer is 6667 nm and thus fulfilling these limitations. The efficiency η of a periodic grating under the scalar approximation is given by

$$\eta(\lambda) = \left|\frac{1}{d}\int_0^d r(x) e^{2\pi i m x/d} dx\right|^2, \tag{5}$$

where $r(x)$ is the reflection function of the blazed grating $r(x) = \sum_{m=-\infty}^{\infty} \delta(x - md) \otimes exp\{2\pi i \frac{h}{\lambda d} \cdot x\}$, with $h \to \lambda_B$. The amplitude of the reflected light of mth order is therefore given by its Fourier transform. Consequently, the efficiency η_m is given by the square of the respective far-field amplitude of the dispersed light [10,12]. For the mth order we find

$$\eta_m(\lambda) = \mathrm{sinc}^2\left(\frac{\lambda_B}{\lambda} - m\right). \tag{6}$$

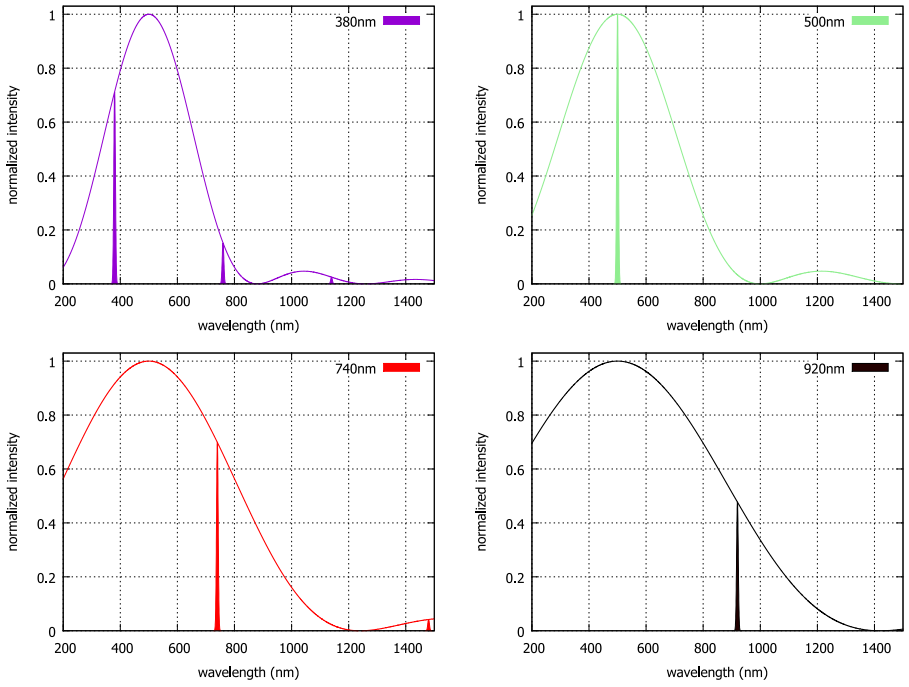

Fig. 1. Monochromatic intensities of various wavelength and their higher order diffraction peaks at the n-fold wavelength in the range between 200 nm and 1500 nm.

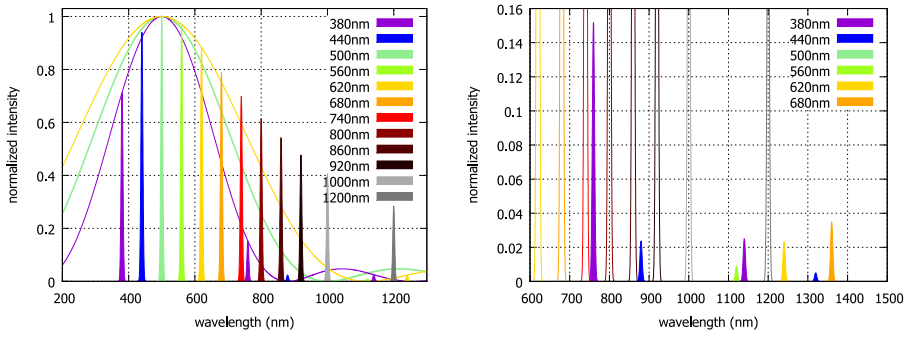

Fig. 2. Left: Attenuation and second diffraction order for light in the range of 380 nm to 1200 nm. Right: First order maxima (empty peaks) and higher order maxima at the n-fold wavelength (full peaks) for various wavelengths.

As an instructive example for the above discussed problem, we measured the emission spectrum of an UV-lamp shown in Fig. 3. Multiples of the main peak at 402 nm can be easily identified. In the present case, the real spectral distribution is not of interest. It would depend also on the absorption of the light guides and on the wavelength dependent detection quantum efficiency of the CCD. We can now normalize the intensity of the spectrum such, that the 402 nm peak touches the calculated envelope function.

As a consequence, the peaks at multiples of 402 nm are touching the calculated envelope function, too. Therefore, these intensities are identified as being higher order diffraction intensities and do not represent emission lines. Therefore, the measured spectrum must be corrected for higher order diffraction prior to the correction for the system response of the detection system (including absorption of the light guides, grating correction and DQE of the CCD detector) in order to retrieve the true emission spectrum of the UV-lamp.

In order to find a correction function for considering multiple diffraction maxima, the amplitude distribution of m diffraction orders in the far-field [9,10] has to be considered. It is the sum over all far-field amplitudes, as shown already in the definition of the reflection function. Consequently, the intensity distribution is the square of the

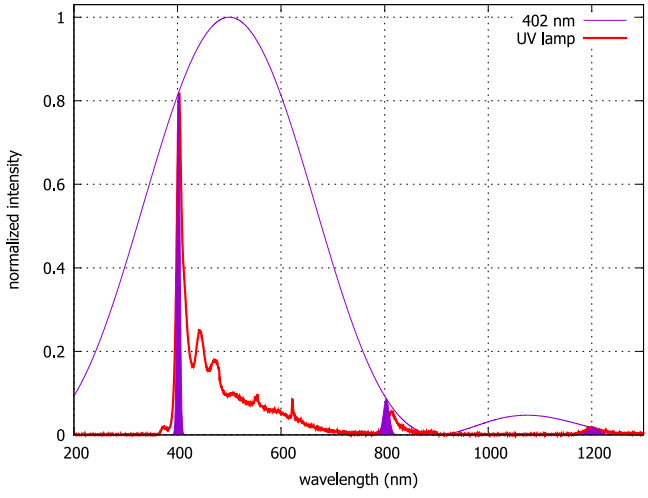

Fig. 3. Emission spectrum of a UV lamp neither with correction for higher diffraction orders nor with absorption correction.

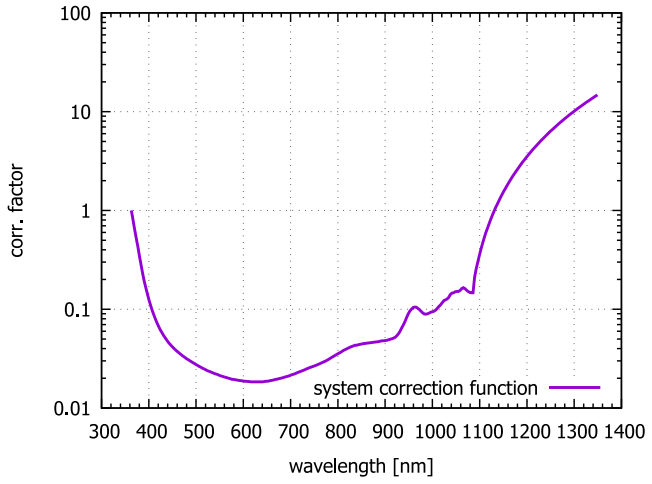

Fig. 4. Experimentally determined system response function (SRF) including reflectivity of the mirrors, the absorption of the light guides and the DQE of the CCD detector. It was measured by using transition radiation of an Al-specimen as light source. It does not consider higher scattering orders.

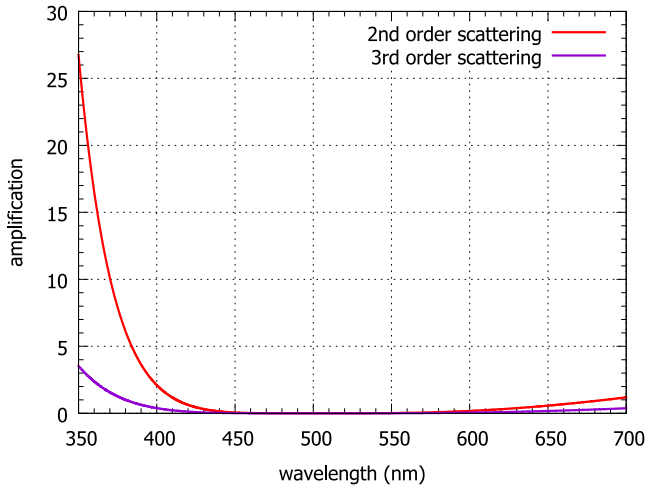

Fig. 5. Correction functions for 2nd- and 3rd-order scattering.

amplitudes. Thus, a correction for higher order diffraction has to include the sum over the detectable orders, which in our case is up to the third order diffraction.

4. The system response function and a correction function for higher-order diffraction

The detected signal intensity $I_d(x)$ at the position x of the detector is the emitted intensity $I_0(\lambda)$ altered by the system response function (SRF(λ)) shown in Fig. 4. It was determined by comparing the theoretical spectrum of transition radiation emitted from a thin Al foil with the experimental counterpart [13,14]. The SRF(λ) itself consists of several functions describing each part of the optical system separately. It therefore contains the reflectivity of the high-grade polished Aluminum mirrors $R(\lambda)$, the optical absorption of the light guiding optical fibers $e^{-\alpha(\lambda)\cdot l}$ – with $\alpha(\lambda)$ being the absorption coefficient and l being the length of the light guides –, the detection quantum efficiency of the CCD array $DQE(\lambda)$ and the grating correction function $k_1(\lambda)$ of the blazed grating, respectively. It can be written as

$$I_d(\lambda) = I_0 \cdot SRF(\lambda) = I_0 \cdot R(\lambda) \cdot e^{-\alpha(\lambda)\cdot l} \cdot DQE(\lambda) \cdot k_1(\lambda) \tag{7}$$

and should read zero at λ_B. But due to the fact that there is a grating loss [15] to be considered a reduction of intensity even at the blazing wavelength is observed.

One property of the blazed grating can already be seen in Fig. 3. All wavelengths except of the blazed wavelength are somewhat attenuated. This attenuation can be corrected with the blazing response function $k_1(\lambda)$, which from now on will be defined as the correction function for the first-order diffraction efficiency of a blazed grating.

$$k_1(\lambda) = 1 - \eta_1(\lambda) = 1 - \mathrm{sinc}^2\left(\frac{\lambda_B}{\lambda} - 1\right) \tag{8}$$

The only problem is that k_1 only applies in cases where the higher diffraction orders lie outside the detected spectral range. Wide bandgap materials that emit blue or ultraviolet light require a correction function for higher order diffraction because their second and third order diffraction might be in the observed spectral range. If this is not taken into account, the second and third order diffraction maxima of a blue emission could be misinterpreted as red and infrared band emissions, respectively. In order to remove higher diffraction orders from the spectrum, a grating response including the intensities I_m of diffraction order m has to be identified. There are no orders of $m \geq 4$ detected by the system, since it is limited in detectable wavelength by the absorption of the optical fibers. Eq. (7) has to be corrected for the effect of the refraction function of the blazed grating (see also Eq. (5)). Thus, the detected spectrum has be written as

$$I_d(\lambda) = R(\lambda) \cdot e^{-\alpha(\lambda)\cdot l} \cdot DQE(\lambda) \cdot \left[\sum_{m=1}^{3} I_m(\lambda) \cdot \mathrm{sinc}^2\left(\frac{\lambda_B}{\lambda} - m\right)\right] \tag{9}$$

The last term in Eq. (9) is the new grating response substituting $k_1(\lambda)$ from Eq. (7). It contains additive terms. Therefore, the single scattering distribution has to be found prior to the correction of the SRF(λ). Thus, the general procedure for carrying out the correction is as follows:

(1) the spectrum of the first diffraction order ($m = 1$) is stretched by multiplying the wavelength axis by the diffraction order m to be corrected.
(2) the stretched spectrum is multiplied by a correction function $f_m(m \cdot \lambda)$, which is described in detail below.
(3) the stretched spectrum multiplied by the correction function is subtracted from the spectral range of the mth diffraction order.
(4) the standard correction routine correcting for R(λ), $e^{-\alpha(\lambda)\cdot l}$, and DQE($\lambda$) is applied finally.

We define the correction function $f_m(m \cdot \lambda)$ as the intensity ratio of mth diffraction order to the first diffraction order

$$f_m(m \cdot \lambda) = \frac{\eta_m(\lambda)}{\eta_1(\lambda)} = \frac{\mathrm{sinc}^2\left(\frac{\lambda_B}{\lambda} - m\right)}{\mathrm{sinc}^2\left(\frac{\lambda_B}{\lambda} - 1\right)}. \tag{10}$$

Due to the fact that only second- and third-order scattering influences the overall shape of the CL spectrum in the experimentally accessible spectral range, only the correction functions f_2, and f_3 need to be considered and are plotted in Fig. 5.

These functions have to be applied to the first order scattering intensities and subsequently rescaled in wavelength by the factor m before being subtracted from the original spectrum. Thereafter the original SRF(λ) is applied to the spectrum.

5. Application to CaO and GaN

Beside measuring interband transitions in phosphorous materials CL is also frequently used for characterizing defect levels in semiconductors and insulators. The correction function for higher-order scattering is applied to CL spectra of CaO and of GaN, respectively. Common to both materials is the high defect density leading to numerous gap

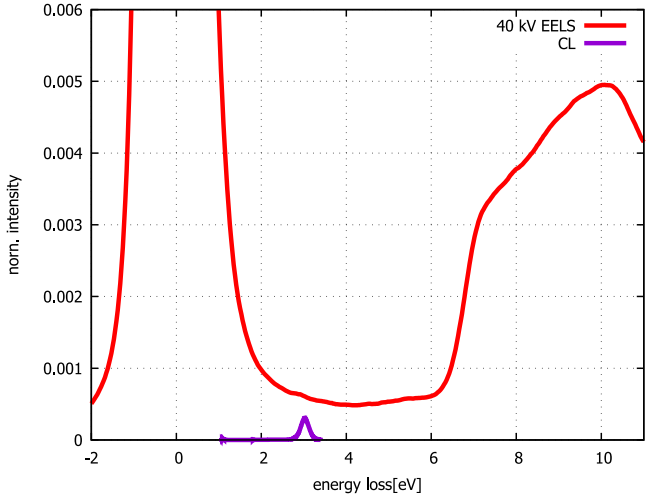

Fig. 6. 40 keV VEELS spectrum of $CaO_{0.98}S_{0.02}$. Gap states at 2.95 eV can be identified. The CL spectrum also shows a strong peak at the respective energy.

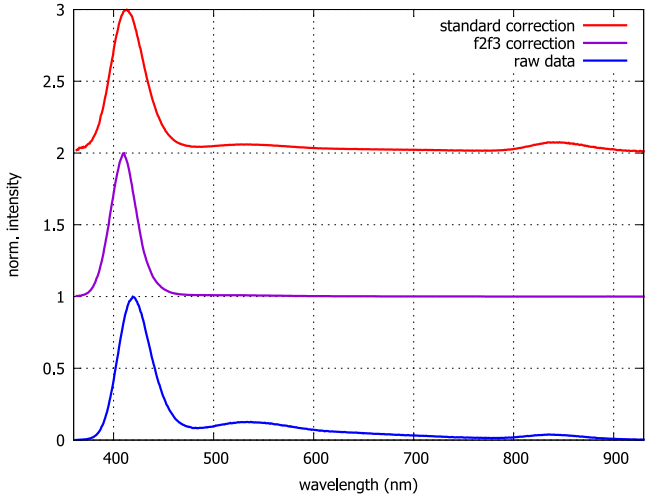

Fig. 7. CL spectrum of $CaO_{0.98}S_{0.02}$ as acquired (bottom), after the f_2f_3-correction prior to the SRF(λ) correction (shifted by 1 for better visibility), and for comparison after the standard correction routine (SRF(λ) only) (shifted by 2 for better visibility).

states. Consequently, signal being non-zero is expected in the mid- and infra-red emission bands, too. Ignoring higher-order scattering of the analyzing grating would lead to intensities at multiples of the original wavelength.

CaO has a band gap of 6.25 eV [16] which was confirmed by means of valence electron energy loss spectrometry (VEELS) and CL performed at 40 keV. The low beam energy was chosen in order to suppress the excitation of Čerenkov radiation and to avoid their corresponding Čerenkov losses. Thus neither in the VEELS spectrum nor in the CL spectrum the Čerenkov effect has to be taken into account [5,17,18]. Additionally, CaO is well known to attract Sulfur. Thus it is used in the production of iron and steel. The specimen used was contaminated with 1% sulfur, which was determined using electron energy loss spectrometry (EELS) and energy dispersive X-ray spectroscopy (EDX). This contamination leads to gap-states being found at 2.95 eV being clearly visible in the VEELS spectrum shown in Fig. 6. For better visibility the CL spectrum is also shown at the base line of the VEELS spectrum. The VEELS spectrum consists of 460 single acquisitions subsequently aligned and summed up in order to reduce noise. There was no further data treatment applied.

Since the gap-states were found at 2.95 eV, a main peak at 421.5 nm is expected in the CL spectrum. Consequently, the second diffraction maximum is therefore found at 843 nm. There is another faint peak at 3.3 eV in the VEELS spectrum, which already out of range for our optical set-up. The absorption coefficient of the light guides damps this wavelength totally. Fig. 7 shows the CL measurements on the $CaO_{0.98}S_{0.02}$ crystal. If the standard correction of the SRF(λ) would be applied, the higher order diffraction peak would be still present in the resulting spectrum. But if the proposed f_2f_3-correction function is applied prior to the standard SRF(λ), this artifact can be successfully removed.

In the case of CaO, there are no intensities emitted having a wavelength of 840 nm. Therefore, the interpretation of the CL spectrum is relatively simple. However, this is not the case for GaN. Due to the defect density, GaN also shows emission in the red region. This is then superimposed with the higher diffraction orders of the blue interband transition. However, the standard routine amplifies signals in the red range because the blazing function f_k requires this. In addition, the DQE correction also requires amplification of the red signal. If only applying the standard correction, the red signal is amplified much too much and the impression is created that there is an additional and particularly strong interband transition there. Fig. 8 shows the CL measurements on a GaN crystal. In order to prevent the sample from

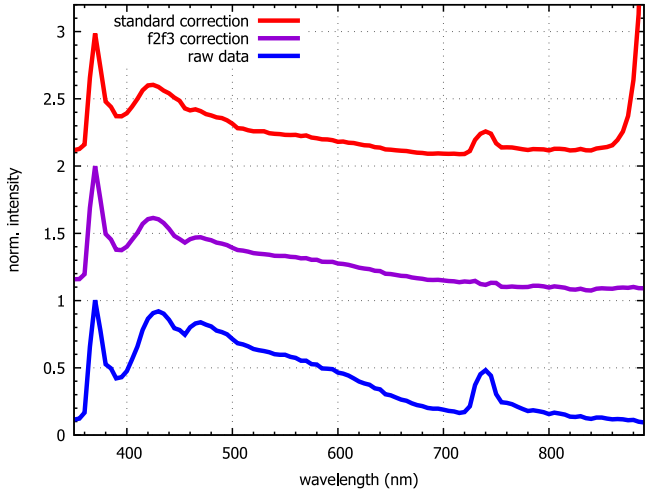

Fig. 8. CL spectrum of GaN as acquired (bottom), after the f_2f_3-correction prior to the SRF(λ) correction (shifted by 1 for better visibility), and for comparison after the standard correction routine (SRF(λ) only) (shifted by 2 for better visibility).

emitting Čerenkov light, the beam energy was chosen to be 45 keV which is well below the Čerenkov limit [19]. Again, the f_2f_3-corrected CL spectrum is shown in the center. The 2nd-order peak at 740 nm is completely removed. Furthermore, no erroneous amplification of the signal is observed above 860 nm. This would be present if only the standard SRF(λ) correction routine would be applied.

6. Conclusion

The f_2f_3 correction presented to remove higher order diffraction artifacts from the measured spectrum is necessary if maxima in the CL spectrum are expected to lie at the lower end of the wavelength scale detectable with the CL system. Such transitions can arise in particular due to the presence of defect states or dopants. Otherwise, the superposition of the higher diffraction orders with signals of longer wavelengths would make the interpretability of CL spectra questionable when using a grating as analyzer.

In general, higher order diffraction appears, as soon as a grating is used for the analysis of any optical spectrum. Consequently, the proposed correction is not limited to CL spectra only, but might have

a much larger field of applications. Higher order diffraction can be avoided when using an optical prism instead. But this would have the draw back of wavelength dependent dispersion leading to a non-linear wavelength-axis of the recorded spectrum.

Declaration of competing interest

I declare no conflict of interest.

Data availability

Data will be made available on request.

Acknowledgments

This research was in part supported by the SINNCE project of the European Union's Horizon 2020 program under the grant agreement No. 810626.

References

[1] T.B. Brown, Brightness of cathodoluminescence at low current densities and low voltages, J. Opt. Soc. Amer. 27 (1937) 186–192.
[2] U. Fano, A theory on cathode luminescence, Phys. Rev. 58 (1940) 544–553.
[3] F.J. Garcia de Abajo, Optical excitations in electron microscopy, Rev. Modern Phys. 82 (2010) 209–275, http://dx.doi.org/10.1103/RevModPhys.82.209.
[4] V.L. Ginzburg, I.M. Frank, On the transition radiation theory, J. Exp. Theor. Phys. 16 (1946) 1–15.
[5] P.A. Čerenkov, Visible emission of clean liquids by action of γ radiation, Dokl. Akad. Nauk. SSSR 2 (1934) 451.
[6] J.M. Lohr, Color photography of luminescence, J. Phys. Chem. 17 (1913) 675–681.
[7] J.T. Griffith, S. Zhang, J. Lhuillier, D. Zhu, W.Y. Fu, A. Howkins, I. Boyd, D. Stowe, D.J. Wallis, C.J. Humphreys, R.A. Oliver, Nano-cathodoluminescence reveals the effect of electron damage on the optical properties of nitride optoelectronics and the damage threshold, J. Appl. Phys. 120 (2016) 165704, http://dx.doi.org/10.1063/1.4965989.
[8] J.E. Harvey, R.N. Pfisterer, Understanding diffraction grating behavior: including conical diffraction and rayleigh anomalies from transmission gratings, Opt. Eng. 58 (2019) 087105, http://dx.doi.org/10.1117/1.OE.58.8.087105.
[9] M. Born, E. Wolf, Principle of Optics, Pergamon Press Ltd., Oxford, England, ISBN: 0-08-026482-4.
[10] G.J. Swanson, Binary Optics Technology: The Theory and Design of Multilevel Diffractive Optical Elements, Technical Report 854, MIT Lincoln Laboratory, Massachusetts, 1989.
[11] J. Francés, C. Neipp, S. Gallego, S. Bleda, A. Márquez, I. Pascual, A. Beléndez, Comparison of simplified theories in the analysis of the diffraction efficiency in surface-relief gratings, in: F. Wyrowski, J.T. Sheridan, J. Tervo, Y. Meuret (Eds.), Optical Modelling and Design II, Proc. of SPIE Vol. 8429, 2012, pp. 8429U–1, http://dx.doi.org/10.1117/12.922332.
[12] F. Languy, K. Fleury, C. Lenaerts, J. Liocq, D. Regaert, T. Thibert, S. Habraken, Flat Fresnel doublets made of PMMA and PC:combining low cost production and very high concentration ratio for CPV, Opt. Express 19 (2011) A280–A294, http://dx.doi.org/10.1364/OE.19.00A280.
[13] M. Stöger-Pollach, K. Bukvišová, S. Schwarz, M. Kvapil, T. Šamoril, M. Horák, Fundamentals of cathodoluminescence in a STEM: The impact of sample geometry and electron beam energy on light emission of semiconductors, Ultramicroscopy 200 (2019) 111–124, http://dx.doi.org/10.1016/j.ultramic.2019.03.001.
[14] M. Stöger-Pollach, C.F. Pichler, T. Dan, G.A. Zickler, K. Bukvišová, O. Eibl, F. Brandstätter, Coherent light emission in cathodoluminescence when using GaAs in a scanning (transmission) electron microscope, Ultramicroscopy 224 (2021) 113260, http://dx.doi.org/10.1016/j.ultramic.2021.113260.
[15] R. Casini, P.G. Nelson, On the intensity distribution function of blazed reflective diffraction gratings, J. Opt. Soc. Amer. A 31 (2014) 2179–2184, http://dx.doi.org/10.1364/JOSAA.31.002179.
[16] E.L. Albuquerque, M.S. Vasconcelos, Structural, electronics and optical properties of CaO, J. Phys. Conf. Ser. 100 (2008) 042006, http://dx.doi.org/10.1088/1742-6596/100/4/042006.
[17] M. Stöger-Pollach, H. Franco, P. Schattschneider, S. Lazar, B. Schaffer, W. Grogger, Z.H. W, Čerenkov losses: a limit for bandgap determination and Kramers–Kronig analysis, Micron 37 (5) (2006) 396–402, http://dx.doi.org/10.1016/j.micron.2006.01.001.
[18] M. Stöger-Pollach, Optical properties and band gaps from low loss EELS: pitfalls and solutions, Micron 39 (2008) 1092–1110, http://dx.doi.org/10.1016/j.micron.2008.01.023.
[19] M. Horak, M. Stöger-Pollach, The Čerenkov limit of Si, GaAs and GaP in electron energy loss spectrometry, Ultramicroscopy 157 (2015) 73–78, http://dx.doi.org/10.1016/j.ultramic.2015.06.005.